Available online at www.sciencedirect.com
ScienceDirect
International Journal of Solids and Structures 45 (2008) 1017–1031
INTERNATIONAL JOURNAL OF SOLIDS AND STRUCTURES
www.elsevier.com/locate/ijsolstr

Controlling parameter of the stress intensity factors for a planar interfacial crack in three-dimensional bimaterials

Nao-Aki Noda [a,*], Chunhui Xu [a,b,1]

[a] Department of Mechanical Engineering, Kyushu Institute of Technology, 1-1, Sensui-cho, Tobata, Kitakyushu 804-8550, Japan
[b] College of Science, China Agricultural University, Beijing 100083, P.R. China

Received 13 November 2006; received in revised form 6 September 2007
Available online 21 September 2007

Abstract

Numerical solutions of singular integral equations are discussed in the analysis of a planar rectangular interfacial crack in three-dimensional bimaterials subjected to tension. The problem is formulated as a system of singular integral equations on the basis of the body force method. In the numerical analysis, unknown body force densities are approximated by the products of the fundamental density functions and power series, where the fundamental density functions are chosen to express singular behavior along the crack front of the interface crack exactly. The calculation shows that the present method gives smooth variations of stress intensity factors along the crack front for various aspect ratios. The present method gives rapidly converging numerical results and highly satisfied boundary conditions throughout the crack boundary. The stress intensity factors are given with varying the material combination and aspect ratio of the crack. It is found that the stress intensity factors K_I and K_{II} are determined by the bimaterial constant ε alone, independent of elastic modulus ratio and Poisson's ratio.

Keywords: Elasticity; Stress intensity factor; Body force method; Interface crack; Singular integral equation

1. Introduction

In recent years, composite materials and adhesive or bonded joints are being used in wide range of engineering field. With the rapidly increasing the use of composite materials and adhesive, much attention has been paid to the interface because the fracture is usually originated from the interfacial region. It is desirable to design and manufacture composite structures whose fracture behavior is known at their interface. Although a lot of studies have been made for interface cracks problems (Comninou, 1977; England, 1965; Erdogan, 1963, 1965; Erdogan and Gupta, 1975; Noda and Oda, 1997; Rice and Sih, 1965; Salganik, 1963; Tucker, 1974; Willis, 1971, 1972), most of these works are on two-dimensional cases. The numerical solutions were

* Corresponding author. Tel./fax: +81 93 884 3124.
E-mail address: noda@mech.kyutech.ac.jp (N.-A. Noda).
[1] Present address: Department of Mechanical Engineering, Kyushu Institute of Technology, 1-1, Sensui-cho, Tobata, Kitakyushu 804-8550, Japan.

0020-7683/$ - see front matter
doi:10.1016/j.ijsolstr.2007.09.013

Notations

$2a \times 2b$ dimensions of rectangular crack
μ_1, μ_2 shear modulus for space 1 and space 2
v_1, v_2 Poisson's ratio for space 1 and space 2
(x, y, z) rectangular coordinate
(ξ, η, ζ) rectangular coordinate (x, y, z) where the body force is applied
ε bimaterial constant $= \frac{1}{2\pi} \ln \left(\frac{\mu_2 \kappa_1 + \mu_1}{\mu_1 \kappa_2 + \mu_2} \right)$
$w_z(\xi,\eta)$, $w_y(\xi,\eta)$, $w_x(\xi,\eta)$ fundamental body force densities to express the stress fields due to a rectangular crack in an infinite body under uniform tension σ_z^∞
$f_{zz}(\xi,\eta)$, $f_{yz}(\xi,\eta)$, $f_{zx}(\xi,\eta)$ unknown body force densities, which are equivalent to the displacement discontinuities
α_i, β_i, γ_i unknown coefficient
(u_x, u_y, u_z) displacement in (x, y, z) direction
$\Delta u_x(x, y)$ crack opening displacement $= u_x(x,y,+0) - u_x(x,y,-0)$
$\Delta u_y(x, y)$ crack opening displacement $= u_y(x,y,+0) - u_y(x,y,-0)$
$\Delta u_z(x, y)$ crack opening displacement $= u_z(x,y,+0) - u_z(x,y,-0)$
K_I, K_{II}, K_{III} stress intensity factors
F_I, F_{II}, F_{III} dimensionless stress intensity factors normalized by $\sigma_z^\infty \sqrt{\pi b}$

discussed in the analysis of a penny-shaped crack between two dissimilar materials (England, 1965; Kassir and Bregman, 1972; Lowengrub and Sneddon, 1974; Mossakovski and Rybka, 1964; Shibuya et al., 1989). Recently, Bercial-Velez et al. (2005) studied a singularly perturbed problem and obtained the asymptotics for the stress intensity factors associated with the perturbation for the crack front. They assumed first to have an interfacial crack with a straight front, and then introduced an in plane perturbation. Chaudhuri (2006) discussed the three-dimensional asymptotic stress field in the vicinity of the circumference of a biomaterial penny-shaped interfacial discontinuity. The finite element method can be applied to practically important 3D interface crack problems (Ikeda et al., 2006; Nagai et al., 2007); however, usually the method was applied to specific material combination. And, therefore, few studies are available if another material combination is necessary. Due to the mathematical difficulties, few analytical methods are available for three-dimensional interface cracks under general material combinations and general aspect ratio. Considering this situation, Noda et al. (2003) evaluated the stress intensity factors of an axi-symmetric interface cracks under torsion and tension by the body force method for general material combinations.

The body force method was originally proposed by Nisitani (1967) as a new method for solving stress concentration problems. In solving crack problems, the body force method uses the stress fields due to a pair of point forces or displacement discontinuities (Nisitani and Murakami, 1974). In those analyses, the problems are formulated as a system of singular integral equations. Then, accurate numerical solutions were investigated in the previous studies (Noda and Oda, 1992; Noda and Matsuo, 1998). For a semi-elliptical surface crack, Noda and Miyoshi (1996) studied the variation of stress intensity factor and crack opening displacement using a hypersingular integral equation, where the unknown body force density was approximated by the products of fundamental density function and polynomial. Here, the fundamental density was chosen to express the stress field due to an elliptical crack in an infinite body exactly. This numerical method was applied to investigate the stress intensity factors of a 3D rectangular crack using the body force method (Wang et al., 2001).

For planar interface crack problems, hypersingular intergro-differential equations were indicated as a general expression (Chen et al., 1999). However, solving the equations is extremely difficult because of the oscillation singularity and overlapping of crack surfaces, both of which are peculiar to interface cracks. In this paper, numerical solutions will be considered for a planar rectangular interface crack on the basis of the equations. Here, the fundamental density functions will be chosen to express singular behavior along the crack front of the interface crack exactly. Then, it will be shown that the smooth variations of stress intensity factor along the crack front are highly satisfactory boundary conditions throughout the crack surface. The influence of the dimension of the interfacial crack and of the ratio of the elastic parameter will be shown completely and exhaustively.

2. Singular integral equations for a planar interfacial crack

Consider two dissimilar elastic half-spaces bonded together along the x–y plane (see Fig. 1(a)) with a fixed rectangular Cartesian coordinate system x_i $(i = x, y, z)$. Suppose that the upper half-space is occupied by an elastic medium with constants $(\mu_1, \ v_1)$, and the lower half-space by an elastic medium with constants (μ_2, v_2). Here, μ_1, μ_2 are shear modulus for space 1 and space 2, and v_1, v_2 are Poisson's ratio for space 1 and space 2. The crack is assumed to be located at the bimaterial interface.

Hypersingular intergro-differential equations for three-dimensional cracks on a bimaterial interface in Fig. 1(a) were derived by Chen et al. (1999) and expressed as shown in Eq. (1).

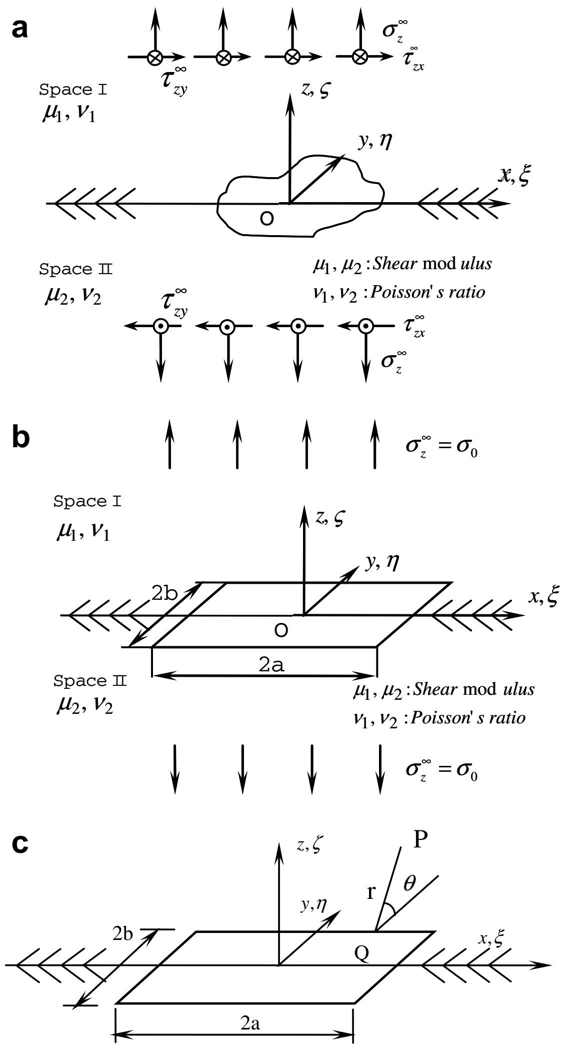

Fig. 1. Problem configuration.

$$\mu_1(\Lambda_2-\Lambda_1)\frac{\partial\Delta u_z(x,y)}{\partial x}+\mu_1\frac{(2\Lambda-\Lambda_1-\Lambda_2)}{2\pi}\int_s\frac{1}{r^3}\Delta u_x(\xi,\eta)\mathrm{d}S(\xi,\eta)$$
$$+3\mu_1\frac{(\Lambda_1+\Lambda_2-\Lambda)}{2\pi}\left\{\int_s\frac{(x-\xi)^2}{r^5}\Delta u_x(\xi,\eta)\mathrm{d}S(\xi,\eta)+\int_s\frac{(x-\xi)(y-\eta)}{r^5}\Delta u_y(\xi,\eta)\mathrm{d}S(\xi,\eta)\right\}=-p_x(x,y) \quad (1a)$$
$$\mu_1(\Lambda_2-\Lambda_1)\frac{\partial\Delta u_z(x,y)}{\partial y}+\mu_1\frac{(2\Lambda-\Lambda_1-\Lambda_2)}{2\pi}\int_s\frac{1}{r^3}\Delta u_y(\xi,\eta)\mathrm{d}S(\xi,\eta)$$
$$+3\mu_1\frac{(\Lambda_1+\Lambda_2-\Lambda)}{2\pi}\left\{\int_s\frac{(x-\xi)(y-\eta)}{r^5}\Delta u_x(\xi,\eta)\mathrm{d}S(\xi,\eta)+\int_s\frac{(y-\eta)^2}{r^5}\Delta u_y(\xi,\eta)\mathrm{d}S(\xi,\eta)\right\}=-p_y(x,y) \quad (1b)$$
$$\mu_1(\Lambda_1-\Lambda_2)\left(\frac{\partial\Delta u_x(x,y)}{\partial x}+\frac{\partial\Delta u_y(x,y)}{\partial y}\right)+\mu_1\frac{(\Lambda_1+\Lambda_2)}{2\pi}\int_s\frac{1}{r^3}\Delta u_z(\xi,\eta)\mathrm{d}S(\xi,\eta)=-p_z(x,y) \quad (1c)$$
$$\Lambda=\frac{\mu_2}{\mu_1+\mu_2},\quad \Lambda_1=\frac{\mu_2}{\mu_1+\kappa_1\mu_2},\quad \Lambda_2=\frac{\mu_2}{\mu_2+\kappa_2\mu_1},$$
$$\kappa_1=3-4v_1,\quad \kappa_2=3-4v_2,\quad r^2=(x-\xi)^2+(y-\eta)^2 \quad (1d)$$
$$(x,y)\in S,\quad S=\{(x,y)||x|\leqslant a,|y|\leqslant b\}$$
$$\Delta u_x(x,y)=u_x(x,y,0^+)-u_x(x,y,0^-)=\sum_{l=1}^{2}\frac{1}{\mu_l}f_{zx}(x,y),$$
$$\Delta u_y(x,y)=u_y(x,y,0^+)-u_y(x,y,0^-)=\sum_{l=1}^{2}\frac{1}{\mu_l}f_{yz}(x,y), \quad (1e)$$
$$\Delta u_z(x,y)=u_z(x,y,0^+)-u_z(x,y,0^-)=\sum_{l=1}^{2}\frac{\kappa_l-1}{\mu_l(\kappa_l+1)}f_{zz}(x,y).$$

In Eq. (1), unknown functions are crack opening displacements, in other words, displacement discontinuities Δu_x, Δu_y, $\Delta\ u_z$ defined in Eq. (1e), which are equivalent to the body force densities $f_{zx}(x,y)$, $f_{yz}(x,y)$, $f_{zz}(x,y)$ as shown in Eq. (1e). Here, (ξ,η,ζ) is a rectangular coordinate (x,y,z) where the displacement discontinuities are distributed. The notations p_x, p_y, p_z denote surface tractions in the x, y, z directions at the crack surface, and τ_{zx}^∞, τ_{yz}^∞, σ_z^∞ are the stresses at infinity. As shown in Fig. 1(b), we can put $\tau_{zx}^\infty=p_x=0$, $\tau_{yz}^\infty=p_y=0$, $\sigma_z^\infty=p_z=\sigma_0$. It is assumed that the bimaterial is subjected to normal stresses $\sigma_{x1}^\infty, \sigma_{x2}^\infty, \sigma_{y1}^\infty, \sigma_{y2}^\infty$, which are parallel to the interface to produce $\varepsilon_{x1}^\infty=\varepsilon_{x2}^\infty, \varepsilon_{y1}^\infty=\varepsilon_{y2}^\infty$, but those normal stresses do not affect the stress intensity factors. Since the integral has a hypersingularity of the form r^{-3} when $x=\xi$ and $y=\eta$, the integration should be interpreted in a sense of a finite part integral in the region S (Hadamard, 1923). Outside the region of S, we may put $\Delta u_x=0$, $\Delta u_y=0$, $\Delta u_z=0$, which mean displacement fields have single-valuedness.

3. Numerical solutions of the singular integral equations

Consider a rectangular interface crack under tension at infinity. In the numerical solution, it is necessary to express the oscillation singular stress, which is specific to the crack tip of interface cracks. For

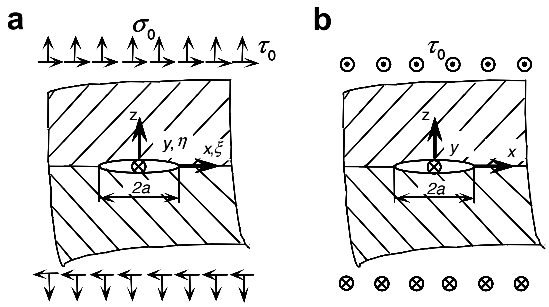

Fig. 2. Fundamental densities for two-dimensional problems.

two-dimensional crack problems (see Fig. 2), crack opening displacement can be expressed in the following equations (Rice and Sih, 1965).

$$\text{For Fig. 2(a)}: \Delta u_z + \mathrm{i}\Delta u_x = \sum_{l=1}^{2}\left\{\frac{\kappa_l - 1}{\mu_l(1+\kappa_l)} w_z(\xi) + \mathrm{i}\frac{1}{\mu_l} w_x(\xi)\right\} \times [\sigma_0 + \mathrm{i}\tau_0]$$
$$= \sum_{l=1}^{2} \frac{1+\kappa_l}{4\mu_l \cosh \pi\varepsilon}\sqrt{a^2-\xi^2}\left(\frac{a-\xi}{a+\xi}\right)^{i\varepsilon} \times [\sigma_0 + \mathrm{i}\tau_0], \tag{2a}$$

$$\text{For Fig. 2(b)}: \Delta u_y = \sum_{l=1}^{2}\frac{1}{\mu_l} w_y(\xi)\tau_0 = \sum_{l=1}^{2}\frac{1}{\mu_l}\frac{1+\kappa_l}{4}\sqrt{a^2-\xi^2}\tau_0 \tag{2b}$$

$$\varepsilon = \frac{1}{2\pi}\ln\left(\frac{\mu_2\kappa_1 + \mu_1}{\mu_1\kappa_2 + \mu_2}\right) \tag{3}$$

$$\kappa_l = \begin{cases} \dfrac{3-v_l}{1+v_l} & \text{plane stress} \\ 3 - 4v_l & \text{plane strain} \end{cases} \quad (l = 1,\ 2) \tag{4}$$

Here, σ_0, τ_0 are the stresses at infinity, and $w_1(\xi)$ and $w_2(\xi)$ are called fundamental density functions, which express stress fields due to a single 2D interface crack exactly (Nisitani et al., 1993).

In the present analysis, the fundamental densities and polynomials have been used to approximate the unknown functions as a continuous function. First, we put

$$\begin{aligned} \Delta u_x(\xi,\eta) &= w_x(\xi,\eta)F_x(\xi,\eta), \\ \Delta u_y(\xi,\eta) &= w_y(\xi,\eta)F_y(\xi,\eta), \\ \Delta u_z(\xi,\eta) &= w_z(\xi,\eta)F_z(\xi,\eta). \end{aligned} \tag{5}$$

Considering Eq. (2), for the three-dimensional interface crack problem, the fundamental density functions are expressed as the follows.

$$\left.\begin{aligned} w_x(\xi,\eta) &= \sum_{l=1}^{2}\frac{1+\kappa_l}{4\mu_l\cosh\pi\varepsilon}\sqrt{a^2-\xi^2}\sqrt{b^2-\eta^2}\sin\left(\varepsilon\ln\left(\frac{a-\xi}{a+\xi}\right)\right) \\ w_y(\xi,\eta) &= \sum_{l=1}^{2}\frac{1+\kappa_l}{4\mu_l\cosh\pi\varepsilon}\sqrt{a^2-\xi^2}\sqrt{b^2-\eta^2}\sin\left(\varepsilon\ln\left(\frac{b-\eta}{b+\eta}\right)\right) \\ w_z(\xi,\eta) &= \sum_{l=1}^{2}\frac{1+\kappa_l}{4\mu_l\cosh\pi\varepsilon}\sqrt{a^2-\xi^2}\sqrt{b^2-\eta^2}\cos\left(\varepsilon\ln\left(\frac{a-\xi}{a+\xi}\right)\right)\cos\left(\varepsilon\ln\left(\frac{b-\eta}{b+\eta}\right)\right) \end{aligned}\right\} \tag{6}$$

The fundamental densities (6) lead to expressing the oscillation stress singularity and overlapping of crack surfaces along the crack front exactly. To satisfy the boundary conditions for the rectangle region of the interface crack, the following expressions may be applied, where the unknowns are coefficients of the polynomials α_i, β_i, γ_i.

$$\begin{aligned} F_x(\xi,\eta) &= \alpha_0 + \alpha_1\eta + \cdots + \alpha_{n-1}\eta^{(n-1)} + \alpha_n\eta^n + \alpha_{n+1}\xi + \alpha_{n+2}\xi\eta + \cdots + \alpha_{2n}\xi\eta^n + \cdots \\ &\quad + \alpha_{l-n-1}\xi^m + \alpha_{l-n}\xi^m\eta + \cdots + \alpha_{l-1}\xi^m\eta^n = \sum_{i=0}^{l-1}\alpha_i G_i(\xi,\eta), \\ F_y(\xi,\eta) &= \beta_0 + \beta_1\eta + \cdots + \beta_{n-1}\eta^{(n-1)} + \beta_n\eta^n + \beta_{n+1}\xi + \beta_{n+2}\xi\eta + \cdots + \beta_{2n}\xi\eta^n + \cdots \\ &\quad + \beta_{l-n-1}\xi^m + \beta_{l-n}\xi^m\eta + \cdots + \beta_{l-1}\xi^m\eta^n = \sum_{i=0}^{l-1}\beta_i G_i(\xi,\eta), \\ F_z(\xi,\eta) &= \gamma_0 + \gamma_1\eta + \cdots + \gamma_{n-1}\eta^{(n-1)} + \gamma_n\eta^n + \gamma_{n+1}\xi + \gamma_{n+2}\xi\eta + \cdots + \gamma_{2n}\xi\eta^n + \cdots \\ &\quad + \gamma_{l-n-1}\xi^m + \gamma_{l-n}\xi^m\eta + \cdots + \gamma_{l-1}\xi^m\eta^n = \sum_{i=0}^{l-1}\gamma_i G_i(\xi,\eta), \\ l &= (m+1)(n+1), \\ G_0(\xi,\eta) &= 1, G_1(\xi,\eta) = \eta, \cdots, G_{n+1}(\xi,\eta) = \xi, \cdots, G_{l-1}(\xi,\eta) = \xi^m\eta^n. \end{aligned} \tag{7}$$

By substituting Eqs. (5)–(7) into Eq. (1), we obtain the following system of algebraic equations for the determination of coefficients α_i, β_i, γ_i, which can be determined by selecting a set of collocation points (Noda et al., 2003; Noda and Miyoshi, 1996).

$$\left.\begin{aligned}
&\sum_{i=0}^{l-1}\alpha_i(f_{x1}^1+f_{x1}^2)+\sum_{i=0}^{l-1}\beta_i f_{y1}+\sum_{i=0}^{l-1}\gamma_i f_{z1}=0\\
&\sum_{i=0}^{l-1}\alpha_i f_{x2}+\sum_{i=0}^{l-1}\beta_i(f_{y2}^1+f_{y2}^2)+\sum_{i=0}^{l-1}\gamma_i f_{z2}=0\\
&\sum_{i=0}^{l-1}\alpha_i f_{x3}+\sum_{i=0}^{l-1}\beta_i f_{y3}+\sum_{i=0}^{l-1}\gamma_i f_{z3}=-p_z
\end{aligned}\right\}\tag{8a}$$

Here,

$$\left.\begin{aligned}
&f_{z1}=\mu_1(\Lambda_2-\Lambda_1)\frac{\partial}{\partial x}w_z(x,y)G_i(x,y)\\
&f_{z2}=\mu_1(\Lambda_2-\Lambda_1)\frac{\partial}{\partial y}w_z(x,y)G_i(x,y)\\
&f_{x3}=\mu_1(\Lambda_2-\Lambda_1)\frac{\partial}{\partial x}w_x(x,y)G_i(x,y)\\
&f_{y3}=\mu_1(\Lambda_2-\Lambda_1)\frac{\partial}{\partial y}w_y(x,y)G_i(x,y)\\
&f_{x1}^1=\mu_1\frac{2\Lambda-\Lambda_1-\Lambda_2}{2\pi}\int_s\frac{1}{r^3}w_x(\xi,\eta)G_i(\xi,\eta)\mathrm{d}S(\xi,\eta)\\
&f_{x1}^2=3\mu_1\frac{\Lambda_1+\Lambda_2-\Lambda}{2\pi}\int_s\frac{(x-\xi)^2}{r^5}w_x(\xi,\eta)G_i(\xi,\eta)\mathrm{d}S(\xi,\eta)\\
&f_{y1}=3\mu_1\frac{\Lambda_1+\Lambda_2-\Lambda}{2\pi}\int_s\frac{(x-\xi)(y-\eta)}{r^5}w_y(\xi,\eta)G_i(\xi,\eta)\mathrm{d}S(\xi,\eta)\\
&f_{y2}^1=\mu_1\frac{2\Lambda-\Lambda_1-\Lambda_2}{2\pi}\int_s\frac{1}{r^3}w_y(\xi,\eta)G_i(\xi,\eta)\mathrm{d}S(\xi,\eta)\\
&f_{x2}=3\mu_1\frac{\Lambda_1+\Lambda_2-\Lambda}{2\pi}\int_s\frac{(x-\xi)(y-\eta)}{r^5}w_x(\xi,\eta)G_i(\xi,\eta)\mathrm{d}S(\xi,\eta)\\
&f_{y2}^2=3\mu_1\frac{\Lambda_1+\Lambda_2-\Lambda}{2\pi}\int_s\frac{(y-\eta)^2}{r^5}w_y(\xi,\eta)G_i(\xi,\eta)\mathrm{d}S(\xi,\eta)\\
&f_{z3}=\mu_1\frac{\Lambda_1+\Lambda_2}{2\pi}\int_s\frac{1}{r^3}w_z(\xi,\eta)G_i(\xi,\eta)\mathrm{d}S(\xi,\eta)
\end{aligned}\right\}\tag{8b}$$

where

$$\begin{aligned}
f_{z1}&=\mu_1(\Lambda_2-\Lambda_1)\sum_{l=1}^{2}\frac{1+\kappa_l}{4\mu_l\cosh\pi\varepsilon}\times\frac{1}{\sqrt{a^2-x^2}}\times x^{-1+m}y^n\sqrt{b^2-y^2}\cos\left(\varepsilon\ln\left(\frac{b-y}{b+y}\right)\right)\\
&\quad\times\left[\left(a^2m-(1+m)x^2\right)\cos\left(\varepsilon\ln\left(\frac{a-x}{a+x}\right)\right)+2a\varepsilon x\sin\left(\varepsilon\ln\left(\frac{a-x}{a+x}\right)\right)\right]\\
f_{z2}&=\mu_1(\Lambda_2-\Lambda_1)\sum_{l=1}^{2}\frac{1+\kappa_l}{4\mu_l\cosh\pi\varepsilon}\times\frac{1}{\sqrt{b^2-y^2}}\times\left(y^{-1+n}x^m\sqrt{a^2-x^2}\cos\left(\varepsilon\ln\left(\frac{a-x}{a+x}\right)\right)\right.\\
&\quad\left.\times\left[\left(b^2n-(1+n)y^2\right)\cos\left(\varepsilon\ln\left(\frac{b-y}{b+y}\right)\right)+2b\varepsilon y\sin\left(\varepsilon\ln\left(\frac{b-y}{b+y}\right)\right)\right]\right)\\
f_{x3}&=\mu_1(\Lambda_2-\Lambda_1)\sum_{l=1}^{2}\frac{1+\kappa_l}{4\mu_l\cosh\pi\varepsilon}\times\frac{1}{\sqrt{a^2-x^2}}\times\left(x^{-1+m}y^n\sqrt{b^2-y^2}\cos\left(\varepsilon\ln\left(\frac{b-y}{b+y}\right)\right)\right.\\
&\quad\left.\times\left[\left(a^2m-(1+m)x^2\right)\sin\left(\varepsilon\ln\left(\frac{a-x}{a+x}\right)\right)-2a\varepsilon x\cos\left(\varepsilon\ln\left(\frac{a-x}{a+x}\right)\right)\right]\right)\\
f_{y2}&=\mu_1(\Lambda_2-\Lambda_1)\sum_{l=1}^{2}\frac{1+\kappa_l}{4\mu_l\cosh\pi\varepsilon}\times\frac{1}{\sqrt{b^2-y^2}}\times\left(y^{-1+n}x^m\sqrt{a^2-x^2}\cos\left(\varepsilon\ln\left(\frac{a-x}{a+x}\right)\right)\right.\\
&\quad\left.\times\left[\left(b^2n-(1+n)y^2\right)\sin\left(\varepsilon\ln\left(\frac{b-y}{b+y}\right)\right)-2b\varepsilon y\cos\left(\varepsilon\ln\left(\frac{b-y}{b+y}\right)\right)\right]\right)
\end{aligned}\tag{8c}$$

4. How to evaluate the hypersingular integrals

Each integral in Eq. (8) has a hypersingularity of the form r^{-3} when $x = \xi$ and $y = \eta$, and it cannot be evaluated in the present form. Using the Taylor's expansion with the local polar coordinates system $\xi - x = r\cos\theta$, $\eta - y = r\sin\theta$ as shown in Fig. 3, the following expressions are given, and they will be applied to evaluate the integral.

$$\sqrt{a^2 - \xi^2} = P_0(x) - (\xi - x)P_1(x) - (\xi - x)^2 P_2(\xi, x) \tag{9a}$$

$$\sqrt{b^2 - \eta^2} = Q_0(y) - (\eta - y)Q_1(y) - (\eta - y)^2 Q_2(\eta, y) \tag{9b}$$

Here

$$P_0(x) = \sqrt{a^2 - \xi^2}, \quad P_1(x) = \frac{x}{\sqrt{a^2 - x^2}},$$

$$P_2(\xi, x) = \frac{\xi + x}{\sqrt{a^2 - x^2}\left(\sqrt{a^2 - \xi^2} + \sqrt{a^2 - x^2}\right)} \times \frac{a^2}{\left(\xi\sqrt{a^2 - x^2} + x\sqrt{a^2 - \xi^2}\right)}$$

$$Q_0(x) = \sqrt{b^2 - \eta^2}, \quad Q_1(y) = \frac{y}{\sqrt{b^2 - y^2}}$$

$$Q_2(\eta, y) = \frac{\eta + y}{\sqrt{b^2 - y^2}\left(\sqrt{b^2 - \eta^2} + \sqrt{b^2 - y^2}\right)} \times \frac{b^2}{\left(\eta\sqrt{b^2 - y^2} + y\sqrt{b^2 - \eta^2}\right)}$$

$$\begin{aligned} \xi^m &= x^m + m x^{m-1}(\xi - x) + \sum_{i=0}^{m-2}\left[(\mathrm{i}+1)\xi^{(m-2-i)}x^i\right](\xi - x)^2 \\ &= b_0(x) + b_1(x)(\xi - x) + b_2(\xi, x)(\xi - x)^2 \end{aligned} \tag{9c}$$

$$\begin{aligned} \eta^n &= x^n + n x^{n-1}(\eta - y) + \sum_{i=0}^{n-2}\left[(\mathrm{i}+1)\eta^{(n-2-i)}y^i\right](\eta - y)^2 \\ &= c_0(y) + c_1(y)(\eta - y) + c_2(\eta, y)(\eta - y)^2 \end{aligned} \tag{9d}$$

$$FC_{11} = \cos\left(\varepsilon \ln\left(\frac{a - \xi}{a + \xi}\right)\right) = R_{01}(x) + R_{11}(x)(\xi - x) + R_{21}(x)(\xi - x)^2 \tag{9e}$$

$$FS_{11} = \sin\left(\varepsilon \ln\left(\frac{a - \xi}{a + \xi}\right)\right) = R_{02}(x) + R_{12}(x)(\xi - x) + R_{22}(x)(\xi - x)^2 \tag{9f}$$

$$FC_{21} = \cos\left(\varepsilon \ln\left(\frac{b - \eta}{b + \eta}\right)\right) = T_{01}(y) + T_{11}(y)(\eta - y) + T_{21}(y)(\eta - y)^2 \tag{9g}$$

$$FS_{21} = \sin\left(\varepsilon \ln\left(\frac{b - \eta}{b + \eta}\right)\right) = T_{02}(y) + T_{12}(y)(\eta - y) + T_{22}(y)(\eta - y)^2 \tag{9h}$$

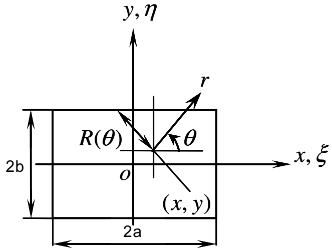

Fig. 3. Integral parameters.

Here

$$R_{01}=\cos\left(\varepsilon\ln\left(\frac{a-x}{a+x}\right)\right),\quad R_{02}=\sin\left(\varepsilon\ln\left(\frac{a-x}{a+x}\right)\right),$$
$$T_{01}=\cos\left(\varepsilon\ln\left(\frac{b-y}{b+y}\right)\right),\quad T_{02}=\sin\left(\varepsilon\ln\left(\frac{b-y}{b+y}\right)\right),$$
$$R_{11}(x)=\frac{2a\varepsilon}{a^2-x^2}R_{02},\quad R_{12}(x)=-\frac{2a\varepsilon}{a^2-x^2}R_{01},\quad T_{11}(y)=\frac{2b\varepsilon}{b^2-y^2}T_{02},\quad T_{12}(y)=-\frac{2b\varepsilon}{b^2-y^2}T_{01},$$
$$R_{21}(x)=\begin{cases}\dfrac{1}{(\xi-x)^2}(FC_{11}-R_{01}(x)-R_{11}(x)(\xi-x)) & |x-\xi|\geqslant\varepsilon_0\\ \dfrac{2a\varepsilon x}{(a^2-x^2)^2}R_{02}-\dfrac{2a^2\varepsilon^2}{(a^2-x^2)^2}R_{01} & |x-\xi|\leqslant\varepsilon_0\end{cases},$$
$$R_{22}(x)=\begin{cases}\dfrac{1}{(\xi-x)^2}(FS_{11}-R_{02}(x)-R_{12}(x)(\xi-x)) & |x-\xi|\geqslant\varepsilon_0\\ \dfrac{2a\varepsilon x}{(a^2-x^2)^2}R_{01}-\dfrac{2a^2\varepsilon^2}{(a^2-x^2)^2}R_{02} & |x-\xi|\leqslant\varepsilon_0\end{cases}\tag{9i}$$
$$T_{21}(y)=\begin{cases}\dfrac{1}{(\eta-y)^2}(FC_{21}-T_{01}(y)-T_{11}(y)(\eta-y)) & |y-\eta|\geqslant\varepsilon_0,\\ \dfrac{2b\varepsilon y}{(b^2-y^2)^2}T_{02}-\dfrac{2b^2\varepsilon^2}{(b^2-y^2)^2}T_{01} & |y-\eta|\leqslant\varepsilon_0\end{cases}$$
$$T_{22}(y)=\begin{cases}\dfrac{1}{(\eta-y)^2}(FS_{21}-T_{02}(y)-T_{12}(y)(\eta-y)) & |y-\eta|\geqslant\varepsilon_0,\\ \dfrac{2b\varepsilon y}{(b^2-y^2)^2}T_{01}-\dfrac{2b^2\varepsilon^2}{(b^2-y^2)^2}T_{02} & |y-\eta|\leqslant\varepsilon_0\end{cases}$$

In the numerical calculation, we may put $\varepsilon_0=10^{-10}$ in Eq. (9i). Using the concept of finite-part integral method and the relations (9a)–(9i), the hypersingular integral in Eq. (8) can be reduced to the following form.

$$\begin{aligned}I_{mn}(x,y)&=\int_0^{2\pi}\int_0^{R(\theta)}\left[\frac{D_0(x,y)}{r^2}+\frac{D_1(\theta)}{r}\right]\mathrm{d}r\mathrm{d}\theta+\int_0^{2\pi}\int_0^{R(\theta)}D_2(r,\theta)\mathrm{d}r\mathrm{d}\theta\\&=\int_0^{2\pi}\left[-\frac{D_0(x,y)}{R(\theta)}+D_1(x,y,\theta)\ln(R(\theta))+\int_0^{R(\theta)}D_2(x,y,r,\theta)\mathrm{d}r\right]\mathrm{d}\theta\end{aligned}\tag{10}$$

In Eq. (10), $D_0(x,y)$, $D_1(x,y,\theta)$ and $D_2(x,y,r,\theta)$ are known functions, which can be expressed as a combination of Eq. (9). Now the integral in (10) is general, and can be calculated numerically. The notation $R(\theta)$ means a distance between a point (x,y) in question and a point on the fictitious boundary of the crack as shown in Fig. 3.

5. Numerical results and discussion

For general cases, the stress intensity factors associated with the three-dimensional planar interface crack front edge are defined as shown in Eq. (11). Here, a local coordinate (r,θ) as shown in Fig. 1(c) is used.

$$\begin{aligned}K(Q)&=K_I(Q)+iK_{II}(Q)=\lim_{r\to0}\sqrt{2\pi r}r^{1/2-i\varepsilon}[\sigma_z(r,\theta)+\mathrm{i}\tau_{zx}(r,\theta)]_{\theta=0}\\&=\frac{\mu_1\mu_2(1+2\mathrm{i}\varepsilon)}{2\cosh\pi\varepsilon}\left(\frac{1}{\mu_1+\kappa_1\mu_2}+\frac{1}{\mu_2+\kappa_2\mu_1}\right)\times\lim_{\xi\to0}[\Delta u_z(r)+\mathrm{i}\Delta u_x(r)]\sqrt{\frac{2\pi}{\xi}}(r)^{-i\varepsilon},\\K_{III}(Q)&=\lim_{r\to0}\sqrt{2\pi r}[\sigma_{yz}(r,\theta)]_{\theta=0}=\frac{\mu_1\mu_2}{2(\mu_1+\mu_2)}\lim_{\xi\to0}\Delta u_y(r)\sqrt{\frac{2\pi}{r}},\\\Delta u_i(r)&=u_i(r,\pi)-u_i(r,-\pi),\quad(i=x,\ y,\ z)\end{aligned}\tag{11}$$

Consider a rectangular interface crack in three-dimensional infinite elastic solid under remote uniform tension $\sigma_z^\infty=1$. By substituting Eqs. (5) and (6) into Eq. (11), the dimensionless factors F_I, F_{II}, F_{III} become as follows.

$$F_I + \mathrm{i}F_{II} = \frac{K_I(x,y)|_{y=\pm b} + \mathrm{i}K_{II}(x,y)|_{y=\pm b}}{\sigma_z^{\infty}\sqrt{\pi b}} = \sqrt{a^2 - x^2}\left(\cos\left(\varepsilon \ln\left(\frac{a-x}{a+x}\right)\right) F_z(x,y)|_{y=\pm b} + 2\mathrm{i}\varepsilon F_y(x,y)|_{y=\pm b}\right)$$

$$F_{III} = \frac{K_{III}(x,y)|_{y=\pm b}}{\sigma_z^{\infty}\sqrt{\pi b}} = \sum_{l=1}^{2} \frac{1+\kappa_l}{4\mu_l \cosh \pi\varepsilon} \frac{1}{(1/\mu_1 + 1/\mu_2)} \sqrt{a^2 - x^2} \sin\left(\varepsilon \ln\left(\frac{a-x}{a+x}\right)\right) F_x|_{y=\pm b} \tag{12}$$

Numerical integrals have been performed very accurately using double exponential type formulas; for example, scientific subroutine library FACOM SSL2 DAQME.

5.1. Compliance of boundary condition and convergence of numerical solutions

Fig. 4(a)–(c) show the compliance of boundary condition along the crack surface for $a/b = 1$, $\nu_1 = \nu_2 = 0.3$, $\varepsilon = 0.02$ when the collocation point number is 100(10 × 10). Here, the boundary conditions are considered at

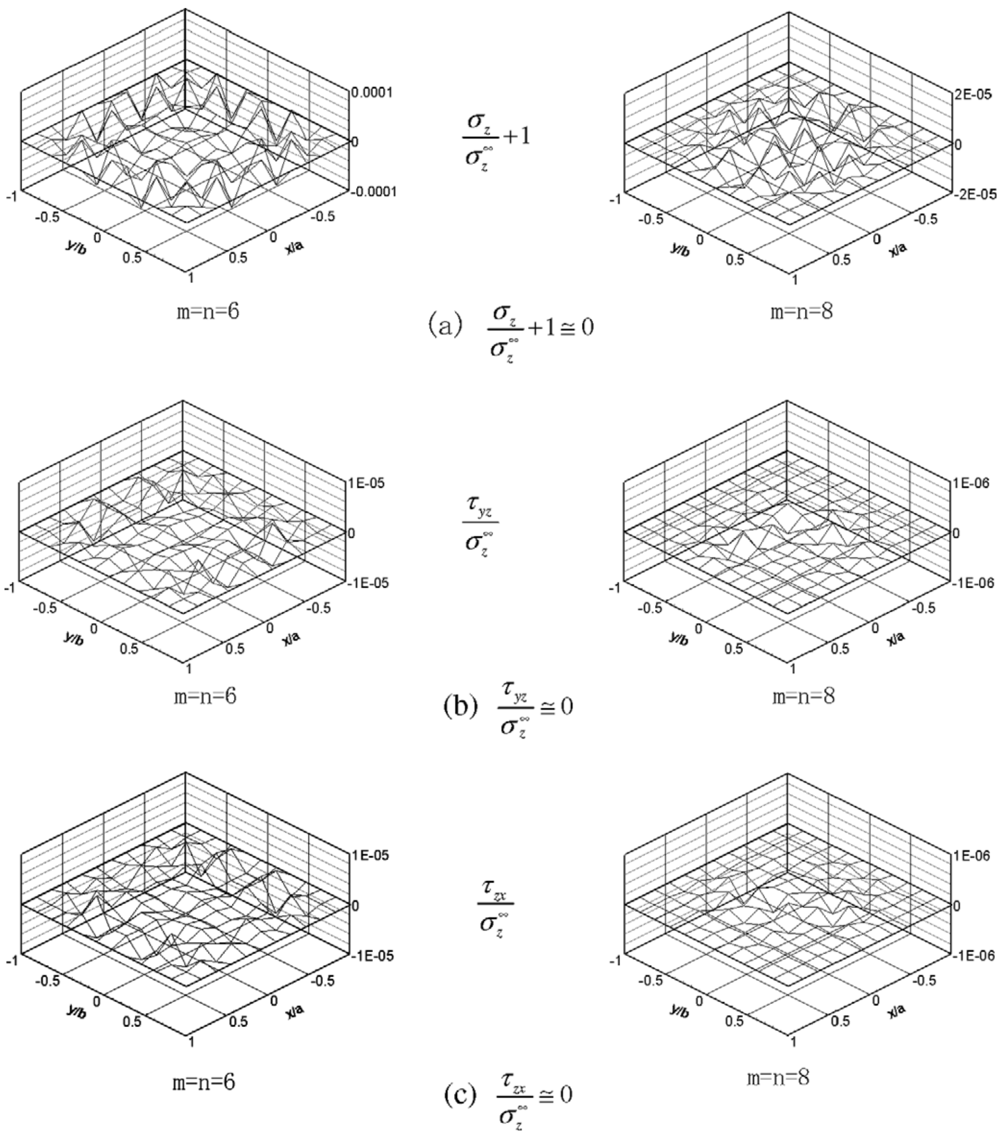

Fig. 4. Compliance of boundary condition for $a/b = 1$, $\varepsilon = 0.02$.

the intersection of the mesh $10 \times 10$when the polynomial exponents m and n in Eq. (8) are changed as $m = n = 6$ and $m = n = 8$. In solving the algebraic Eq. (8), the least square regression method is applied to minimize the residual stress at the collocation points. It is seen that the remaining stresses $(\sigma_z/\sigma_z^\infty + 1)$, $\tau_{yz}/\sigma_z^\infty$, $\tau_{zx}/\sigma_z^\infty$ on the fictitious boundary of the crack are less than 4.4×10^{-5} when $m = n = 6$, less than 1.5×10^{-6}, when $m = n = 8$.

For the crack in homogeneous materials, the results of dimensionless stress intensity factors are shown in Table 1 with varying the polynomial exponents when the collocation point is 10×10, $a/b = 1$, $\nu_1 = \nu_2 = 0.3$. The results coincide with the previous results given by Wang et al. (2001) and Qin and Noda (2003). Table 2 shows the results of $\varepsilon = 0.02$ when the collocation point is 10×10, a/b=1, and $\nu_1 = \nu_2 = 0.3$. From Tables 1 and 2, it is seen that the present method gives the results with good convergence.

5.2. Comparison with the two-dimensional case

For large aspect ratio a/b, the results should coincide with the two-dimensional solution. For $a/b = 8$ the stress intensity factors are given in Table 3 when the polynomial exponents $m = n = 8$ and the collocation point number is 10×10. It is seen that the present results coincide with the two-dimensional exact solution known as $F_I = 1$, $F_{II} = 2\varepsilon$, $F_{III} = 0$ when $a/b \to \infty$.

5.3. Solutions for general cases

For general cases, the following results are given. Here, the polynomial exponents are taken as $m = n = 8$ with the collocation point number 10×10. The distributions of the stress intensity factor F_I and F_{II} are shown in Table 4 with varying ε when $a/b = 1$. It is seen that the stress intensity factor F_I decreases with increasing ε, and F_{II} increases with increasing of ε. The maximum stress intensity factors are compared with the results of a penny-shaped interface crack in Table 5. For ordinary cracks, ε=0, it is known that the stress intensity factor of a square crack is larger than the one of a penny-shaped crack with the same dimension. In Table 5, F_I values

Table 1
Convergence of stress intensity factor F_I at $y = b$ for $\varepsilon = 0$, $a/b = 1$

x/a	0/11	1/11	2/11	3/11	4/11	5/11	6/11	7/11	8/11	9/11	10/11
$m = n = 4$	0.7521	0.7507	0.7462	0.7379	0.7250	0.7066	0.6821	0.6509	0.6108	0.5538	0.4497
$m = n = 6$	0.7538	0.7520	0.7467	0.7377	0.7248	0.7072	0.6836	0.6520	0.6094	0.5482	0.4423
$m = n = 8$	0.7534	0.7516	0.7463	0.7373	0.7243	0.7063	0.6821	0.6500	0.6081	0.5513	0.4543
Qin	0.7534	0.7512	0.7462	0.7379	0.7255	0.7072	0.6821	0.6497	0.6090	0.5521	0.4464
Wang	0.7534	0.7517	0.7465	0.7376	0.7245	0.7066	0.6828	0.6512	0.6086	0.5492	0.4536

Table 2
Convergence of stress intensity factor at $y = b$ for $\varepsilon = 0.02$, $a/b = 1$

x/a	0/11	1/11	2/11	3/11	4/11	5/11	6/11	7/11	8/11	9/11	10/11
(a) Stress intensity factor F_I											
$m = n = 4$	0.7531	0.7512	0.7457	0.7364	0.7233	0.7059	0.6828	0.6517	0.6073	0.5385	0.4177
$m = n = 6$	0.7524	0.7507	0.7456	0.7367	0.7237	0.7060	0.6826	0.6519	0.6098	0.5465	0.4329
$m = n = 8$	0.7528	0.7511	0.7459	0.7369	0.7238	0.7058	0.6822	0.6514	0.6099	0.5490	0.4400
(b) Stress intensity factor F_{II}											
$m = n = 4$	0.0272	0.0271	0.0268	0.0264	0.0257	0.0248	0.0236	0.0221	0.0200	0.0171	0.0127
$m = n = 6$	0.0273	0.0272	0.0270	0.0265	0.0259	0.0250	0.0238	0.0223	0.0203	0.0174	0.0131
$m = n = 8$	0.0274	0.0273	0.0271	0.0266	0.0260	0.0251	0.0239	0.0224	0.0203	0.0176	0.0133
(c) Stress intensity factor F_{III}											
$m = n = 4$	0	0.0010	0.0021	0.0031	0.0042	0.0053	0.0065	0.0079	0.0094	0.0109	0.0120
$m = n = 6$	0	0.0010	0.0020	0.0031	0.0041	0.0052	0.0064	0.0076	0.0091	0.0106	0.0120
$m = n = 8$	0	0.0010	0.0020	0.0031	0.0041	0.0051	0.0063	0.0075	0.0089	0.0105	0.0120

Table 3
Dimensionless stress intensity factor at $y = b$ or $a/b = 8$

x/a	0/11	1/11	2/11	3/11	4/11	5/11	6/11	7/11	8/11	9/11	10/11
(a) Stress intensity factor F_I											
$\varepsilon = 0.02$	0.9947	0.9946	0.9942	0.9933	0.9917	0.9888	0.9838	0.9750	0.9580	0.9175	0.7954
$\varepsilon = 0.04$	0.9938	0.9937	0.9932	0.9923	0.9907	0.9878	0.9828	0.9739	0.9568	0.9160	0.7931
$\varepsilon = 0.06$	0.9920	0.9919	0.9914	0.9905	0.9889	0.9860	0.9809	0.9719	0.9545	0.9134	0.7892
$\varepsilon = 0.08$	0.9891	0.9890	0.9885	0.9875	0.9859	0.9830	0.9779	0.9687	0.9509	0.9092	0.7836
$\varepsilon = 0.10$	0.9848	0.9847	0.9842	0.9833	0.9816	0.9786	0.9733	0.9640	0.9461	0.9037	0.7755
(b) Stress intensity factor F_{II}											
$\varepsilon = 0.02$	0.0397	0.0397	0.0396	0.0396	0.0395	0.0394	0.0391	0.0387	0.0378	0.0359	0.0304
$\varepsilon = 0.04$	0.0786	0.0786	0.0785	0.0784	0.0783	0.0780	0.0775	0.0766	0.0749	0.0711	0.0601
$\varepsilon = 0.06$	0.1160	0.1160	0.1160	0.1158	0.1156	0.1152	0.1144	0.1131	0.1106	0.1047	0.0885
$\varepsilon = 0.08$	0.1515	0.1515	0.1514	0.1512	0.1509	0.1503	0.1493	0.1476	0.1442	0.1364	0.1151
$\varepsilon = 0.10$	0.1845	0.1845	0.1844	0.1842	0.1838	0.1831	0.1819	0.1797	0.1755	0.1658	0.1394
(c) Stress intensity factor $F_{III} \times 10^2$											
$\varepsilon = 0.02$	0	0.0609	0.1217	0.1823	0.2423	0.3013	0.3584	0.4118	0.4579	0.4793	0.4887
$\varepsilon = 0.04$	0	0.1086	0.2371	0.3551	0.4721	0.5872	0.6985	0.8028	0.8932	0.9370	0.9540
$\varepsilon = 0.06$	0	0.1704	0.3406	0.5101	0.6784	0.8439	1.004	1.155	1.286	1.354	1.375
$\varepsilon = 0.08$	0	0.2141	0.4279	0.6411	0.8562	1.061	1.263	1.453	1.620	1.714	1.736
$\varepsilon = 0.10$	0	0.2484	0.4965	0.7439	0.9897	1.232	1.467	1.690	1.886	2.009	2.026

Table 4
Stress intensity factor at $y = b$ for $a/b = 1$, $\nu_1 = \nu_2 = 0.3$

x/a	0/11	1/11	2/11	3/11	4/11	5/11	6/11	7/11	8/11	9/11	10/11
(a) Stress intensity factor F_I											
$\varepsilon = 0$	0.7534	0.7516	0.7463	0.7373	0.7243	0.7063	0.6821	0.6500	0.6081	0.5513	0.4543
$\varepsilon = 0.02$	0.7528	0.7511	0.7459	0.7369	0.7238	0.7058	0.6822	0.6514	0.6099	0.5490	0.4400
$\varepsilon = 0.04$	0.7509	0.7492	0.7440	0.7351	0.7219	0.7040	0.6804	0.6495	0.6080	0.5470	0.4377
$\varepsilon = 0.06$	0.7478	0.7461	0.7409	0.7320	0.7188	0.7009	0.6773	0.6464	0.6048	0.5436	0.4339
$\varepsilon = 0.08$	0.7433	0.7416	0.7364	0.7275	0.7143	0.6965	0.6729	0.6419	0.6003	0.5389	0.4286
$\varepsilon = 0.10$	0.7373	0.7356	0.7304	0.7215	0.7085	0.6906	0.6671	0.6362	0.5945	0.5329	0.4218
(b) Stress intensity factor F_{II}											
$\varepsilon = 0.02$	0.0274	0.0273	0.0271	0.0266	0.0260	0.0251	0.0239	0.0224	0.0204	0.0176	0.0133
$\varepsilon = 0.04$	0.0542	0.0540	0.0535	0.0527	0.0514	0.0497	0.0474	0.0443	0.0403	0.0349	0.0365
$\varepsilon = 0.06$	0.0798	0.0796	0.0789	0.0777	0.0758	0.0733	0.0699	0.0654	0.0595	0.0515	0.0392
$\varepsilon = 0.08$	0.1040	0.1037	0.1028	0.1012	0.0988	0.0955	0.0911	0.0853	0.0776	0.0673	0.0514
$\varepsilon = 0.10$	0.1263	0.1259	0.1248	0.1229	0.1201	0.1161	0.1107	0.1037	0.0945	0.0821	0.0629

Table 5
Comparison with the results of a penny-shaped interface crack ($\nu_1 = \nu_2 = 0.3$)

	F_I		F_{II}	
	Square	Penny	Square	Penny
$\varepsilon = 0$	0.7534	0.6366	0	0
$\varepsilon = 0.02$	0.7528	0.6364	0.0274	0.0304
$\varepsilon = 0.04$	0.7509	0.6359	0.0542	0.0608
$\varepsilon = 0.06$	0.7478	0.6350	0.0799	0.0912
$\varepsilon = 0.08$	0.7433	0.6338	0.1040	0.1216
$\varepsilon = 0.10$	0.7373	0.6322	0.1263	0.1520

of a square interface crack are also larger than the results of a penny-shaped interface crack, but F_{II} values are smaller. With increasing the value of ε, F_I value of a square interface crack decreases larger, but F_{II} value increases smaller compared with the results of a penny-shaped interface crack. The maximum stress intensity

Table 6
Dimensionless stress intensity factor F_I and F_{II} at the point $(x, y) = (0, b)$ in Fig. 1(b)

	F_I				F_{II}			
	$a/b = 1$	$a/b = 2$	$a/b = 4$	$a/b = 8$	$a/b = 1$	$a/b = 2$	$a/b = 4$	$a/b = 8$
$\varepsilon = 0$	0.7534	0.906	0.977	0.996	0	0	0	0
$\varepsilon = 0.02$	0.7528	0.905	0.976	0.995	0.027	0.035	0.039	0.040
$\varepsilon = 0.04$	0.7509	0.904	0.975	0.994	0.054	0.070	0.077	0.079
$\varepsilon = 0.06$	0.7478	0.901	0.973	0.992	0.080	0.103	0.113	0.116
$\varepsilon = 0.08$	0.7433	0.898	0.970	0.989	0.104	0.134	0.148	0.152
$\varepsilon = 0.10$	0.7373	0.892	0.965	0.985	0.126	0.163	0.180	0.185

factor F_I and F_{II} for a rectangular interface crack at the point $(x, y) = (0, b)$ are given in Table 6 for $a/b = 1$, 2, 4, 8.

5.4. Stress intensity factors are controlled by ε alone

In the previous studies it is seen that the stress intensity factors for interface cracks are controlled by bimaterial constant ε just for two-dimensional interface crack and axisymmetric interface crack (Noda et al., 2003). However, nobody has proved that this conclusion can be applied to general aspect ratio of interface cracks. The stress intensity factors F_I, F_{II}, F_{III} are indicated in Table 7 for $a/b = 1$ and $\varepsilon = 0.02$ for various Poisson's ratio and shear modulus ratio.

Also, the results for a/b=1 and $\varepsilon = 0.04$ are indicated in Table 8, and the results for $a/b = 2$ and $\varepsilon = 0.02$ are given in Table 9. From these tables, it is found that F_I and F_{II} values are constant and independent of the shear modulus ratio μ_2/μ_1 and Poisson's ratio if ε is constant. In other words, the stress intensity factors K_I and K_{II} of planer interface cracks in bimaterials are determined by the bimaterial constant ε alone, independent of the shear modulus ratio and Poisson's ratio, and of course, Young's modulus ratio. The F_{III} values is smaller than the values F_I and F_{II}, and in the range, $F_{III\max} \leqslant 10^{-2} \times F_{I\max}$, and $F_{III\max} \leqslant 0.5 \times F_{II\max}$. The maximum value of F_{III} appears at a point that is very close to the corner of the rectangle.

6. Conclusions

In this study a planar rectangular interfacial crack in three-dimensional bimaterials was considered through the singular integral equations on the basis of the body force method. The conclusion can be summarized as follows:

(1) The unknown functions of the singular integral equations are approximated by using fundamental density functions and polynomials. Here, the fundamental densities are chosen to express the singular behavior of the stresses around the crack front exactly. The numerical results show that this numerical technique is successful, and the boundary conditions are satisfied precisely.
(2) It is seen that the present method gives the results with good convergence. For the large aspect ratio $a/b \geqslant 8$, the stress intensity factors at the center of the crack front coincide with the two-dimension results. The results for homogeneous materials coincide with the previous solutions.
(3) Dimensionless stress intensity factors F_I and F_{II} were found to be constant for the variation of the shear modulus ratio μ_2/μ_1 and Poisson's ratio ν_1, $\nu_2 = 0$–0.5, if ε is constant. In other words, the stress intensity factors K_I and K_{II} of planar interface cracks in bimaterials are determined by the bimaterial constant ε alone, independent of the shear modulus ratio and Poisson's ratio, and of course, Young's modulus ratio.
(4) The F_{III} values is smaller than the values F_I and F_{II}, and in the range, $F_{III\max} \leqslant 10^{-2} \times F_{I\max}$, and $F_{III\max} \leqslant 0.5 \times F_{II\max}$. The maximum value of F_{III} appears at a point that is very close to the corner of the rectangle.

Table 7
Stress intensity factor at $y = b$ for $a/b = 1$, $\varepsilon = 0.02$

ν_1	ν_2	μ_2/μ_1	0/11	1/11	2/11	3/11	4/11	5/11	6/11	7/11	8/11	9/11	10/11
(a) Stress intensity factor F_I													
0	0	1.2870	0.7528	0.7511	0.7459	0.7370	0.7238	0.7059	0.6822	0.6513	0.6099	0.5490	0.4400
0	0.1	1.0439	0.7528	0.7511	0.7459	0.7369	0.7238	0.7059	0.6822	0.6513	0.6099	0.5490	0.4400
0	0.2	0.8009	0.7528	0.7511	0.7459	0.7369	0.7238	0.7058	0.6822	0.6513	0.6099	0.5490	0.4400
0	0.3	0.5578	0.7528	0.7511	0.7459	0.7369	0.7238	0.7058	0.6822	0.6514	0.6099	0.5490	0.4400
0	0.4	0.3148	0.7528	0.7511	0.7459	0.7369	0.7238	0.7058	0.6822	0.6514	0.6099	0.5490	0.4400
0	0.5	0.0718	0.7527	0.7511	0.7459	0.7369	0.7238	0.7058	0.6822	0.6514	0.6099	0.5490	0.4400
0.1	0.1	1.3288	0.7528	0.7511	0.7459	0.7369	0.7238	0.7059	0.6822	0.6514	0.6099	0.5490	0.4400
0.1	0.2	1.0194	0.7528	0.7511	0.7459	0.7369	0.7238	0.7058	0.6822	0.6514	0.6099	0.5490	0.4400
0.1	0.3	0.7101	0.7528	0.7511	0.7459	0.7369	0.7238	0.7058	0.6822	0.6514	0.6099	0.5490	0.4400
0.1	0.4	0.4007	0.7528	0.7511	0.7459	0.7369	0.7238	0.7058	0.6822	0.6514	0.6099	0.5490	0.4400
0.1	0.5	0.0913	0.7527	0.7511	0.7459	0.7369	0.7238	0.7058	0.6822	0.6514	0.6099	0.5490	0.4400
0.2	0.2	1.4019	0.7528	0.7511	0.7459	0.7369	0.7238	0.7058	0.6822	0.6514	0.6099	0.5490	0.4400
0.2	0.3	0.9765	0.7528	0.7511	0.7459	0.7369	0.7238	0.7058	0.6822	0.6514	0.6099	0.5490	0.4400
0.2	0.4	0.5510	0.7528	0.7511	0.7459	0.7369	0.7238	0.7058	0.6822	0.6514	0.6099	0.5490	0.4400
0.2	0.5	0.1256	0.7527	0.7511	0.7459	0.7369	0.7238	0.7058	0.6822	0.6514	0.6099	0.5490	0.4400
0.3	0.3	1.5628	0.7528	0.7511	0.7459	0.7369	0.7238	0.7058	0.6822	0.6514	0.6099	0.5490	0.4400
0.3	0.4	0.8819	0.7528	0.7511	0.7459	0.7369	0.7238	0.7058	0.6822	0.6514	0.6099	0.5490	0.4400
0.3	0.5	0.2010	0.7527	0.7511	0.7459	0.7369	0.7238	0.7058	0.6822	0.6514	0.6099	0.5490	0.4400
0.4	0.4	2.2076	0.7527	0.7511	0.7459	0.7369	0.7238	0.7058	0.6822	0.6514	0.6099	0.5490	0.4400
0.4	0.5	0.5032	0.7527	0.7511	0.7459	0.7369	0.7238	0.7058	0.6822	0.6514	0.6099	0.5490	0.4400
0.4999	0.4999	→0	0.7527	0.7511	0.7459	0.7369	0.7328	0.7058	0.6822	0.6514	0.6099	0.5490	0.4400
(b) Stress intensity factor F_{II}													
0	0	1.2870	0.0278	0.0277	0.0274	0.0269	0.0262	0.0253	0.0241	0.0224	0.0202	0.0171	0.0122
0	0.1	1.0439	0.0277	0.0277	0.0274	0.0269	0.0262	0.0253	0.0241	0.0224	0.0203	0.0172	0.0124
0	0.2	0.8009	0.0277	0.0276	0.0273	0.0268	0.0262	0.0252	0.0240	0.0224	0.0203	0.0173	0.0126
0	0.3	0.5578	0.0276	0.0275	0.0272	0.0268	0.0260	0.0252	0.0240	0.0224	0.0203	0.0174	0.0129
0	0.4	0.3148	0.0274	0.0273	0.0271	0.0266	0.0260	0.0251	0.0239	0.0224	0.0204	0.0176	0.0134
0	0.5	0.0718	0.0271	0.0270	0.0268	0.0264	0.0258	0.0250	0.0238	0.0223	0.0204	0.0178	0.0141
0.1	0.1	1.3288	0.0277	0.0276	0.0273	0.0268	0.0262	0.0252	0.0240	0.0224	0.0203	0.0173	0.0126
0.1	0.2	1.0194	0.0276	0.0275	0.0273	0.0268	0.0261	0.0252	0.0240	0.0224	0.0203	0.0173	0.0127
0.1	0.3	0.7101	0.0275	0.0274	0.0272	0.0267	0.0261	0.0252	0.0240	0.0224	0.0203	0.0174	0.0130
0.1	0.4	0.4007	0.0274	0.0273	0.0270	0.0266	0.0260	0.0251	0.0239	0.0224	0.0204	0.0176	0.0134
0.1	0.5	0.0913	0.0271	0.0270	0.0268	0.0264	0.0258	0.0250	0.0238	0.0223	0.0204	0.0178	0.0141
0.2	0.2	1.4019	0.0275	0.0274	0.0272	0.0267	0.0261	0.0252	0.0240	0.0224	0.0203	0.0174	0.0129
0.2	0.3	0.9765	0.0275	0.0274	0.0271	0.0267	0.0260	0.0251	0.0240	0.0224	0.0204	0.0175	0.0131
0.2	0.4	0.5510	0.0273	0.0272	0.0270	0.0266	0.0260	0.0251	0.0239	0.0224	0.0204	0.0176	0.0135
0.2	0.5	0.1256	0.0271	0.0270	0.0268	0.0264	0.0258	0.0250	0.0238	0.0223	0.0203	0.0178	0.0141
0.3	0.3	1.5628	0.0274	0.0273	0.0271	0.0266	0.0260	0.0251	0.0239	0.0224	0.0204	0.0176	0.0134
0.3	0.4	0.8819	0.0273	0.0272	0.0270	0.0266	0.0259	0.0251	0.0239	0.0224	0.0204	0.0177	0.0136
0.3	0.5	0.2010	0.0271	0.0270	0.0268	0.0264	0.0258	0.0250	0.0238	0.0223	0.0204	0.0178	0.0141
0.4	0.4	2.2076	0.0272	0.0271	0.0269	0.0265	0.0259	0.0250	0.0239	0.0224	0.0204	0.0177	0.0138
0.4	0.5	0.5032	0.0271	0.0270	0.0268	0.0264	0.0258	0.0250	0.0238	0.0223	0.0204	0.0178	0.0141
0.4999	0.4999	→0	0.0271	0.0270	0.0268	0.0264	0.0258	0.0250	0.0238	0.0223	0.0204	0.0178	0.0141
(c) Stress intensity factor $F_{III} \times 10^2$													
0.3	0.3	1.5628	0	0.1010	0.2028	0.3061	0.4115	0.5199	0.6331	0.7545	0.8913	1.051	1.204
0.0	0.5	0.0718	0	0.0869	0.1746	0.2637	0.3550	0.4500	0.5517	0.6662	0.8011	0.9592	1.099
0.0	0.0	1.2870	0	0.1204	0.2415	0.3641	0.4884	0.6141	0.7400	0.8667	1.000	1.156	1.328

Table 8
Stress intensity factor for $a/b = 2$, $\varepsilon = 0.02$

ν_1	ν_2	μ_2/μ_1	0/11	1/11	2/11	3/11	4/11	5/11	6/11	7/11	8/11	9/11	10/11
(a) Stress intensity factor F_I													
0.3	0.3	1.5628	0.9052	0.9038	0.8993	0.8912	0.8791	0.8618	0.8381	0.8057	0.7601	0.6899	0.5583
0	0.5	0.0718	0.9052	0.9038	0.8992	0.8912	0.8791	0.8618	0.8381	0.8057	0.7601	0.6900	0.5584
0	0	1.2870	0.9053	0.9038	0.8993	0.8913	0.8791	0.8619	0.8381	0.8057	0.7601	0.6899	0.5582
(b) Stress intensity factor F_{II}													
0.3	0.3	1.5628	0.0352	0.0351	0.0349	0.0345	0.0338	0.0330	0.0318	0.0302	0.0280	0.0246	0.0189
0	0.5	0.0718	0.0349	0.0348	0.0346	0.0342	0.0336	0.0328	0.0317	0.0301	0.0280	0.0248	0.0193
0	0	1.2870	0.0355	0.0355	0.0352	0.0348	0.0342	0.0333	0.0320	0.0303	0.0279	0.0242	0.0182

Table 9
Stress intensity factor for $a/b = 1$, $\varepsilon = 0.04$

ν_1	ν_2	μ_2/μ_1	0/11	1/11	2/11	3/11	4/11	5/11	6/11	7/11	8/11	9/11	10/11
(a) Stress intensity factor F_I													
0.3	0.3	2.5557	0.7509	0.7492	0.7440	0.7351	0.7219	0.7040	0.6804	0.6495	0.6080	0.5470	0.4377
0	0.5	0.1667	0.7508	0.7492	0.7440	0.7350	0.7219	0.7040	0.6804	0.6495	0.6081	0.5471	0.4378
0	0	1.6667	0.7511	0.7494	0.7442	0.7352	0.7220	0.7040	0.6804	0.6494	0.6079	0.5468	0.4376
(b) Stress intensity factor F_{II}													
0.3	0.3	2.5557	0.0542	0.0540	0.0535	0.0527	0.0514	0.0497	0.0474	0.0443	0.0403	0.0348	0.0265
0	0.5	0.1667	0.0537	0.0535	0.0531	0.0523	0.0511	0.0495	0.0472	0.0442	0.0403	0.0353	0.0277
0	0	1.6667	0.0550	0.0548	0.0543	0.0533	0.0519	0.0501	0.0476	0.0444	0.0401	0.0339	0.0243

Acknowledgements

This research was partly supported by Japanese Government (Monbukagakusho) Scholarship. The authors express our thanks to the member of their group, especially Mr. Yasushi Takase, who carried our much of constructional works.

References

Bercial-Velez, J.P., Antipov, Y.A., Movchan, A.B., 2005. The high order asymptotics and perturbation problems for 3D interfacial cracks. Journal of the Mechanics and Physics of Solids 53, 1128–1162.

Chaudhuri, R.A., 2006. Three dimensional asymptotic stress field in the vicinity of the circumference of a bimaterial penny-shaped interfacial discontinuity. International Journal of Fracture 141, 211–225.

Chen, M.C., Noda, N.A., Tang, R.J., 1999. Application of finite-part integrals to planar interfacial fracture problems in three dimensional bimaterials. Transaction of the ASME Journal of Applied Mechanics 66, 885–890.

Comninou, M., 1977. The interface crack. Transaction of the ASME Journal of Applied Mechanics 44, 631–636.

England, A.H., 1965. A crack between dissimilar media. Transaction of the ASME Journal of Applied Mechanics 32, 400–402.

Erdogan, F., 1963. Stresses distribution in a non-homogeneous elastic plane with crack. Transaction of the ASME Journal of Applied Mechanics 30, 232–236.

Erdogan, F., 1965. Stress distribution in bonded dissimilar materials containing circular or ring-shaped cavities. Transaction of the ASME Journal of Applied Mechanics 32, 403–410.

Erdogan, F., Gupta, G.D., 1975. Bonded wedges with an interface crack under anti-plane shear loading. International Journal of Fracture 11, 583–593.

Hadamard, J., 1923. Lectures on Cauchy's problem in linear partial differential equations. Yale University Press, New Haven, CT.

Kassir, M.K., Bregman, A.M., 1972. The stress intensity factor for a penny-shaped crack between two dissimilar materials. Transaction of the ASME Journal of Applied Mechanics 39, 308–310.

Lowengrub, M., Sneddon, I.N., 1974. The effect of internal pressure on a penny-shaped crack at the interface of two bonded dissimilar elastic half-spaces. International Journal of Engineering Science 12, 387–396.

Ikeda, T., Nagai, M., Yamanaga, K., Miyazaki, N., 2006. Stress intensity factor analyses of interface cracks between dissimilar anisotropic materials using the finite element method. Engineering Fracture Mechanics 73, 2067–2079.

Mossakovski, V.I., Rybka, M.T., 1964. Generalization of the Griffith-Senddon criterion for the case of a non-homogeneous body. Prikladnaia Metematica i Mekhanika 28, 1061–1069.

Nagai, M., Ikeda, T., Miyazaki, N., 2007. Stress intensity factor analysis of a three dimensional interface crack between dissimilar anisotropic materials. Engineering Fracture Mechanics 74, 2481–2497.

Nisitani, H., 1967. The two-dimensional stress problem solved using an electric digital computer. Journal of the Japan Society of Mechanical Engineers 11, 627–632 (in Japanese) [1968. Bulletin of Japan Society of Mechanical Engineers 11, 14–23].

Nisitani, H., Murakami, Y., 1974. Stress intensity factor of an elliptical crack and a semi-elliptical crack in plates subjected to tension. International Journal of Fracture 10, 353–368.

Nisitani, H., Saimoto, A., Noguchi, H., 1993. Analysis of an interface crack based on the body force method. Journal of the Japan Society of Mechanical Engineers, Series A 59, 68–73 (in Japanese).

Noda, N.A., Kagita, M., Chen, M.C., 2003. Analysis of stress intensity factors of a ring-shaped interface crack. International Journal of Solids and Structures 40, 6577–6592.

Noda, N.A., Matsuo, T., 1998. Singular integral equation method for interaction between elliptical inclusions. Transaction of the ASME Journal of Applied Mechanics 65, 310–319.

Noda, N.A., Oda, K., 1992. Numerical solutions of the singular integral equations in the crack analysis using the body force method. International Journal of Fracture 58, 285–304.

Noda, N.A., Miyoshi, S., 1996. Variation of stress intensity factors and crack opening displacement of semi-elliptical surface crack. International Journal of Fracture 75, 19–48.

Noda, N.A., Oda, K., 1997. Interaction effect of stress intensity factors for any number of collinear interface cracks. International Journal of Fracture 84, 117–128.

Qin, T.Y., Noda, N.A., 2003. Stress intensity factors of rectangular crack meeting a bimaterial interface. International Journal of Solids and Structures 40, 2473–2486.

Rice, J.R., Sih, G.C., 1965. Plane problems of cracks in dissimilar media. Transaction of the ASME Journal of Applied Mechanics 32, 418–423.

Salganik, R.L., 1963. The brittle fracture of cemented bodies. Prikladnaia Metematica i Mekhanika 27, 957–962.

Shibuya, T., Koizumi, T., Iwamoto, T., 1989. Stress analysis of the vicinity of an elliptical crack at the interface of two bonded half-spaces. Journal of the Japan Society of Mechanical Engineers 32, 485–491.

Tucker, M.O., 1974. In two-phase solids under longitudinal shear loading. International Journal of Fracture 10, 323–336.

Willis, J.R., 1971. Fracture mechanics of interfacial crack. Journal of the Mechanics and Physics of Solids 19, 353–368.

Willis, J.R., 1972. The penny-shaped crack on an interface. Journal of Mechanics and Applied Mathematics 25, 367–385.

Wang, Q., Noda, N.A., Honda, M., Chen, M.C., 2001. Variation of stress intensity factor along the front of 3D rectangular crack by using a singular integral equation method. International Journal of Fracture 108, 119–131.